Chapter 3

Nonlinear Optical Effects at Ferroelectric Domain Walls

Xin Chen, Wieslaw Krolikowski and Yan Sheng

Additional information is available at the end of the chapter

http://dx.doi.org/10.5772/intechopen.77238

Abstract

Ferroelectric materials tend to form macroscopic domains of electric polarization. These domains have different orientations and coexist in the medium being separated by domain walls. In general, symmetry and structure of ferroelectric domain walls differ from their parent materials and consequently lead to abundant physical properties. In this book chapter, we review the nonlinear optical effects which are bundled with ferroelectric domain walls or whose properties can be significantly enhanced by the presence of domain walls. In particular, we have reviewed Google Scholar articles from 2008 to 2018 using the keywords "nonlinear Čerenkov radiation from ferroelectrics". We show that the spatially steep modulation of the second-order nonlinear optical coefficient across the domain wall leads to strong emission of the Čerenkov second harmonic in bulk materials. This feature also enables an effective nondestructive method for three-dimensional visualization and diagnostics of ferroelectric domain structures with very high resolution and high contrast.

Keywords: ferroelectric domain wall, second harmonic generation, nonlinear Čerenkov radiation, nonlinear diffraction, optical imaging

1. Introduction

The ferroelectric phenomenon was discovered in 1921 by J. Valasek during an investigation of the anomalous dielectric properties of Rochelle salt, $NaKC_4H_4O_6 \cdot 4H_2O$ [1]. During the last few decades, the group of ferroelectric materials has been extended to over 250 pure materials and many more mixed crystal systems. They are intensively investigated because of a wide range of actual and potential applications of ferroelectric in critical fields such as electronics, nonvolatile memories, photonics, photovoltaics, etc. [2–8]. The ferroelectric materials generally consist of small uniform regions in which the spontaneous polarization points to the same

direction, called ferroelectric domains. The interfaces separating different domains in a crystal are called domain walls. For example, there are "180° walls" separating domains with oppositely orientated polarizations and "90° walls" separating regions with mutually perpendicular polarizations. The ferroelectric domain walls have symmetry and structure different from their parent materials and consequently possess many various physical properties including huge conductivity and anomalous dielectric responses [4–7].

Lithium niobate ($LiNbO_3$) is a ferroelectric crystal with important photonics applications thanks to its excellent electro-optic, acousto-optic, and nonlinear optical properties. The crystal supports two distinct orientations of the spontaneous polarization along its optical (*z*) axis, i.e., only 180° domains exist in $LiNbO_3$ crystals. Most importantly for nonlinear optical applications, the ferroelectric domains in $LiNbO_3$ crystal can be periodically aligned by using external stimuli such as external electric field [9] or intense light field [10–13]. The alternative orientations of spontaneous polarization amounts to a spatial modulation of the second-order nonlinear coefficient of the crystal, an essential condition of the so-called quasi-phase-matching (QPM) technique, where the phase mismatch of a nonlinear optical process is compensated by one of the resulting reciprocal lattice vectors induced by the nonlinearity modulation. In the simplest case of second harmonic generation (SHG) in the medium, the quasi-phase-matching condition (which is equivalent to conservation of the momentum of interacting waves) can be expressed as $k_2 - 2k_1 = G$, where k_2 and k_1 represent wave vectors of the second harmonic and fundamental waves, respectively. *G* is the magnitude of the reciprocal vector of the nonlinearity grating.

It has been recently reported that efficient second-order nonlinear optical effects can also occur in an extreme case where only a single-domain wall was involved [14–16]. In fact the steep change of the second-order (χ^2) nonlinearity across the domain wall gives rise for the appearance of the so-called nonlinear Čerenkov radiation, whose emission angle is defined by the longitudinal phase-matching condition [17]. In case of frequency doubling via the Čerenkov second harmonic generation (ČSHG), the second harmonic signal is observed at the angle θ_C defined as $k_2 \cos\theta_C - 2k_1 = 0$ [see **Figure 1(a)**]. The nonlinear Čerenkov interaction has been intensively investigated recently to fully understand all aspects of this fundamental

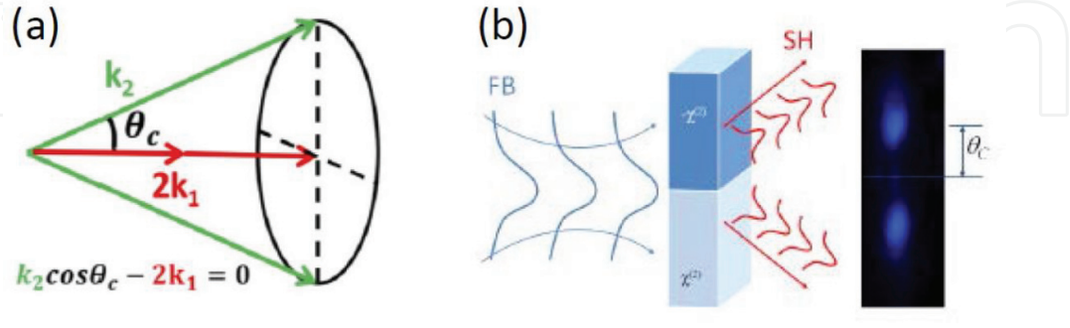

Figure 1. (a) The phase-matching diagram of Čerenkov-type second harmonic generation, where the harmonic emission angle is determined by the longitudinal phase-matching condition, i.e., $k_2 \cos\theta_C - 2k_1 = 0$. (b) Illustration of an experimental observation of the Čerenkov second harmonic generation at a single ferroelectric domain wall. FB, fundamental beam, and SH, second harmonic; represent the second-order nonlinear coefficient of the material [15].

phenomenon and also because of a number of important actual and potential applications in nonlinear optical microscopy [18, 19], ultrashort pulse characterization [20], high harmonic generations [21], and functional materials analysis [22].

In this chapter we review the latest research achievements in both experimental and theoretical studies of the nonlinear Čerenkov interactions that are closely associated with the existence of ferroelectric domain walls. In particular, we discuss two situations, namely, the nonlinear effects arising from a single ferroelectric domain wall and those coming from the multiple domain walls. We solve nonlinear coupled equations for the second harmonic generation and show how the efficiency of these nonlinear interactions depends on the structures of ferroelectric domain patterns and conditions of fundamental wave. These results are important for better understanding of second-order nonlinear optics and inspire optimizing the process for practical applications.

2. Approach and methodology

The authors of this book chapter have been active in the field of nonlinear Čerenkov radiation from domain-engineered ferroelectric crystals for many years. Their latest research outcomes constitute the main body of this review. More details about these research works are available in the authors' publications, which have been correctly cited in the "References." Meanwhile, the authors have also reviewed other research groups' Google Scholar articles on this topic and have included some milestones in this chapter. These research progresses are organized into two categories according to the number of ferroelectric domain walls involved in the interaction, namely, the nonlinear Čerenkov radiations from a single-domain wall and those from multiple walls. In each category, not only experimental research but also theoretical treatment (using, e.g., the standard fast Fourier-transform-based beam propagation method) have been presented.

3. Čerenkov-type second harmonic generation from a single ferroelectric domain wall

The experimental generation of the Čerenkov second harmonic is schematically illustrated in **Figure 1(b)**. The fundamental beam (FB) generally propagates along a ferroelectric domain wall. A pair of beams at doubled frequency, i.e., the second harmonic (SH), is observed in the far field. Their emission angle agrees with that defined by the longitudinal phase-matching condition, i.e., as $\theta_C = \cos^{-1}(2k_1/k_2) = \cos^{-1}(n_1/n_2)$, where n_1 and n_2 are refractive indices of the fundamental and second harmonic waves, respectively. It is clear that the Čerenkov angle depends strongly on material properties. It is worth noting that the efficiency of Čerenkov harmonic generation in a single-domain (homogeneous $\chi^{(2)}$) crystals is low and its experimental observations have been scarce. As we show below, the emission of Čerenkov signal can be strongly enhanced by the presence of ferroelectric domain wall in the beam illuminated area.

For a better understanding of the Čerenkov-type second harmonic generation at a single ferroelectric domain walls, the nonlinear optical interactions from a material system consisting of semi-infinite regions with different quadratic nonlinear responses $\chi^{(2)}$ and $\tilde{\chi}^{(2)}$, as shown in **Figure 2(a)**, are treated both numerically and analytically. We assume the fundamental Gaussian beam (wavelength λ_1 and beam width w) propagates along the boundary separating both media. To avoid any possible influence of the discontinuity in the linear polarization, the refractive index of the system is assumed to be homogenous.

The interaction of the fundamental and second harmonic waves in the nonlinear optical medium is described by the following system of coupled wave equations [23]:

$$\begin{aligned}\frac{\partial E_1}{\partial z} &= \frac{i}{2k_1}\nabla_\perp^2 E_1 - i\frac{\omega_1^2\chi^{(2)}(x)}{k_1c^2}E_1^* E_2 e^{i(k_2-2k_1)z},\\ \frac{\partial E_2}{\partial z} &= \frac{i}{2k_2}\nabla_\perp^2 E_2 - i\frac{\omega_2^2\chi^{(2)}(x)}{2k_2c^2}E_1^2 e^{i(2k_1-k_2)z}.\end{aligned} \tag{1}$$

In these equations ω_1 and $\omega_2 = 2\omega_1$ are the fundamental and SH frequencies, respectively. We assumed that the field can be decomposed into a superposition of these two frequencies, with stationary envelopes and fast oscillating term:

$$E = E_1(x,z)e^{i(k_1z-\omega_1t)} + E_2(x,z)e^{i(k_2z-\omega_2t)} + c.c. \tag{2}$$

Here only the contributions from the diffraction and the quadratic nonlinearity are included, and no transient behavior or interface enhanced linear and/or nonlinear effects are considered.

We numerically solve the Eq. (1) by using the standard fast-Fourier-transform-based beam propagation method. We use the dispersion data of $LiNbO_3$ crystal [24] in simulations. In **Figure 3**, we depict the far-field SH distributions versus the propagation distance, calculated with the fundamental beam propagating along two types of $\chi^{(2)}$ boundary in nonlinear media. **Figure 3(a)** shows the SHG when the nonlinearity changes its sign across the boundary, i.e., $\chi^{(2)} = -\tilde{\chi}^{(2)} = \chi_0^{(2)}$. The strong emission of Čerenkov SHG is observed around 28.6° for the

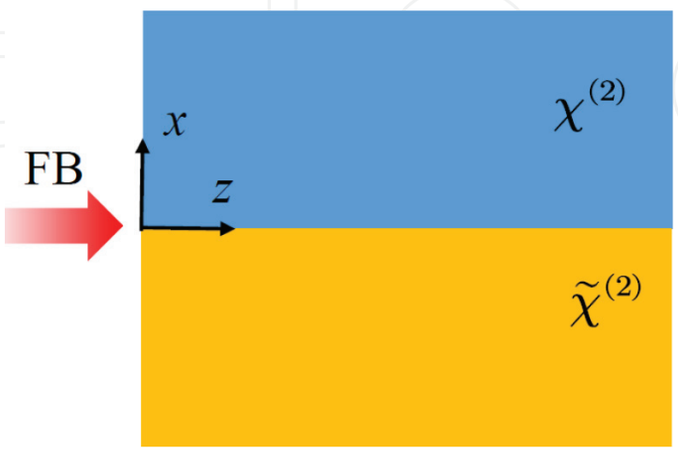

Figure 2. Schematic of the simulation with second harmonic generation in optical media containing two layers of different nonlinear optical responses: $\chi^{(2)}$ and $\tilde{\chi}^{(2)}$.

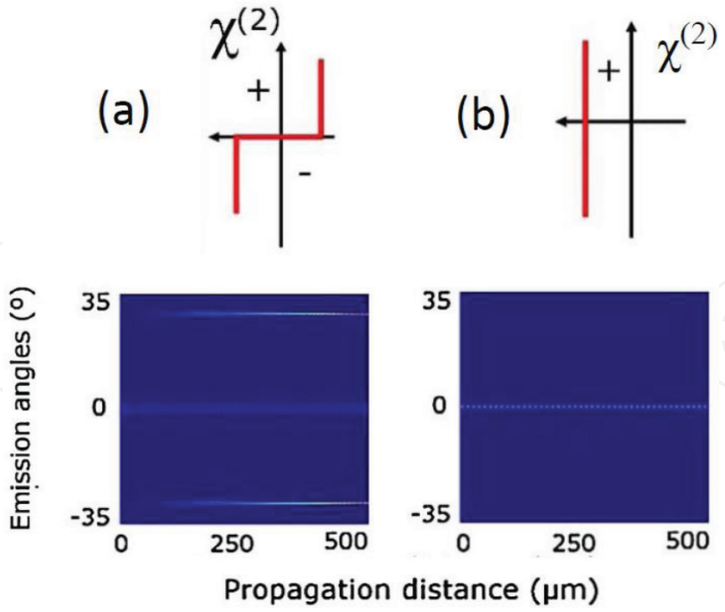

Figure 3. Far-field intensity of the second harmonic generation in composite media with fundamental beam propagating (a) along ferroelectric domain wall and (b) in a homogeneous $\chi^{(2)}$ medium.

fundamental wavelength $\lambda_1 = 1.2 \ \mu m$, in a good agreement with the calculated Čerenkov angle for the $LiNbO_3$ [24]. It is clearly seen that the Čerenkov signal grows monotonically with the interaction distance, which is a typical feature of the longitudinally phase-matched nonlinear interactions. This simulation represents the experimental generation of nonlinear Čerenkov radiation on a single ferroelectric domain wall, across which the second-order nonlinear coefficient alters its sign. In **Figure 3(b)**, we show the calculated SHG in a homogenous $\chi^{(2)}$ medium, i.e. $\chi^{(2)} = \tilde{\chi}^{(2)} = \chi_0^{(2)}$. In this situation only the phase-mismatched, forward second harmonic signal is present. There is no trace of noncollinear Čerenkov harmonic signal. Compared with results shown in **Figure 3(a)**, we confirm the presence of a sharp spatial variation of the $\chi^{(2)}$ nonlinearity forms a sufficient condition for efficient nonlinear Čerenkov radiation.

The behavior becomes even clearer if we analytically deal with the frequency conversion process assuming the undepleted fundamental beam. In this case from Eq. (1), we can obtain the following formula to describe the strength of the nonlinear Čerenkov signal [15]:

$$E_{SH} \propto z \int_{-\infty}^{+\infty} \chi^{(2)}(x) E_1^2(x,z) e^{ik_c x} dx, \tag{3}$$

in which k_c represents the transverse component of the Čerenkov second harmonic wave vector. According to Eq. (3) the amplitude of the Čerenkov signal is defined by the Fourier transform of the product of nonlinearity distribution function $\chi^{(2)}(x)$ and the spatial distribution of the squared amplitude of the fundamental wave $E_1^2(x,z)$. Eq. (3) takes large value as long as its kernel undergoes a fast spatial variation. There are two ways to satisfy this condition. The first is to employ a spatial variation of the second-order nonlinearity $\chi^{(2)}$ in the transverse direction, e.g., propagating the fundamental wave along a ferroelectric domain wall [as shown in **Figure 3(a)**]. The other is to impose a strong spatial confinement to the fundamental beam, namely, to create

a spatially confined $E_1^2(x,z)$. This agrees with the presence of Čerenkov harmonic signal with an assumption of the well-defined rectangular profile of the fundamental beam in [25]. Similar effect was also reported in [26], which shows that a non-diffracting Bessel fundamental beam can lead to nonlinear Čerenkov radiation in a homogeneous crystal.

3.1. Nonlinear diffraction from multiple ferroelectric domain walls

When the fundamental beam is wide enough to cover multiple ferroelectric domain walls, the second harmonic shows more complicated far-field intensity distribution. In fact each domain wall can contribute toward its own Čerenkov second harmonic, and these harmonics will interfere with each other, leading to the so-called nonlinear diffraction [27]. As shown in **Figure 4(a)**, the second harmonic pattern in this case generally consists of two types of spots [15]: (i) peripheral Čerenkov harmonic spots, situated relatively far from the fundamental beam at both sides of the diffraction pattern (top and bottom pairs in the figure), and (ii) central diffraction spots, grouped around the pump position, which is called nonlinear Raman-Nath diffraction, because of its close analogy to the linear Raman-Nath diffraction from a dielectric grating.

In fact Eq. (3) can still be used to calculate the Čerenkov second harmonic from multiple ferroelectric domain walls, except that the $\chi^{(2)}(x)$ is now a periodic function of spatial variable [28]. For 1D periodic domain pattern, the function $\chi^{(2)}(x)$ can be expressed as the following Fourier series:

$$\chi^{(2)}(x) = \sum_{m=0,\,\pm1,\,\pm2} g_m e^{imG_0X}. \tag{4}$$

Here $G_0 = 2\pi/\Lambda$ is the primary reciprocal lattice vector (Λ is the modulation period of $\chi^{(2)}$ grating), the coefficients $g_m\,(m \neq 0) = 2\sin(\pi mD)/\pi m$ and $g_0 = 2D - 1$ with D being the duty cycle defined by the ratio of the length of the positive domains to the period of the $\chi^{(2)}$ structure. Considering a fundamental Gaussian beam, i.e., $E_1(x) = e^{-(x-x_0)^2/a^2}$ (with a being the beam width and x_0 denoting the central position of the beam), the integral in Eq. (3) can be evaluated as

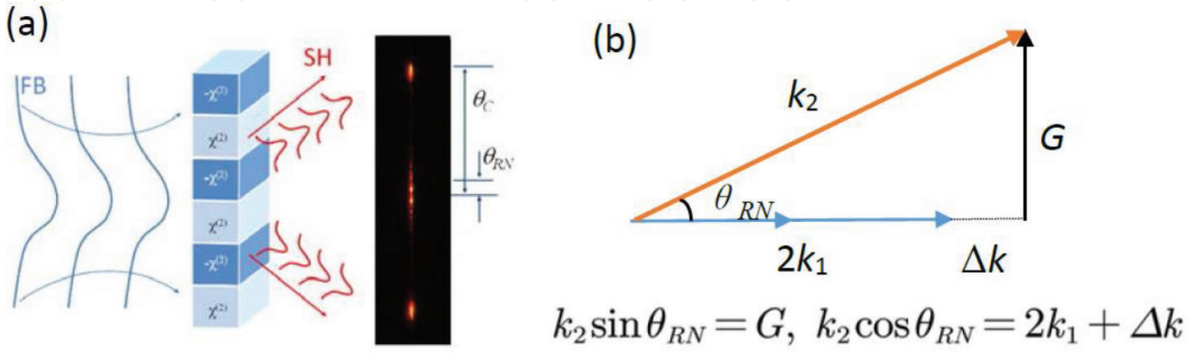

Figure 4. (a) Scheme of Čerenkov SH emission in a 1D periodically poled $LiNbO_3$ crystal. The right inset shows experimentally recorded far-field second harmonic image. The SH spots at small angles (θ_{RN}) represent the Raman-Nath emission, while the spot at bigger angles θ_C is the Čerenkov second harmonics [15]. (b) The phase-matching diagram of the nonlinear Raman-Nath diffraction, which satisfies only the transverse phase-matching condition $k_2 \sin\theta_{RN} = G$.

$$\int \chi^{(2)}(x) E_1^2(x) e^{ik_c x} dx = a(\pi/2)^{1/2} \times \sum_{m=0,\pm1,\pm2,\ldots} g_m e^{-a^2(mG_0+k_c)^2/8} e^{i(mG_0+k_c)x_0}. \quad (5)$$

According to the definition of the Čerenkov second harmonic generation, the variation of the fundamental wavelength leads to the harmonic emission at different angles, i.e. the spatial frequency k_c in Eq. (5) changes. As a result, the intensity of the Čerenkov second harmonic signal varies as well considering the fact that different k_c corresponds to different Fourier coefficients g_m. In **Figure 5**, we show the wavelength response, i.e., the value $|E_{SH}|^2$ of the Čerenkov SH generated by the fundamental Gaussian wave with different beam widths (a). When a wide fundamental beam is used, for instance, a = 60 μm, the strength of the Čerenkov signal is very sensitive to the wavelength, showing a series of intensity peaks [see **Figure 5(a)**]. The emission is quite strong at these peak wavelengths (e.g., at λ_1 = 1.108 μm) but falls dramatically at the others (e.g., at λ_1 = 1.038 μm). Such a sensitive dependence of the Čerenkov second harmonic intensity on the fundamental wavelength is a typical characteristic of light interference in the case of multiple domain walls. It is very interesting to see that, depending on the value of beam width a, the wavelength tuning shows weaker dependence on the wavelength, namely, the less contribution from the interference effect. Finally when the width of the fundamental beam becomes so narrow that it covers only a single-domain wall (e.g., a = 2 μm), all second harmonic peaks disappear, and the Čerenkov intensity exhibits monotonic dependence on wavelength.

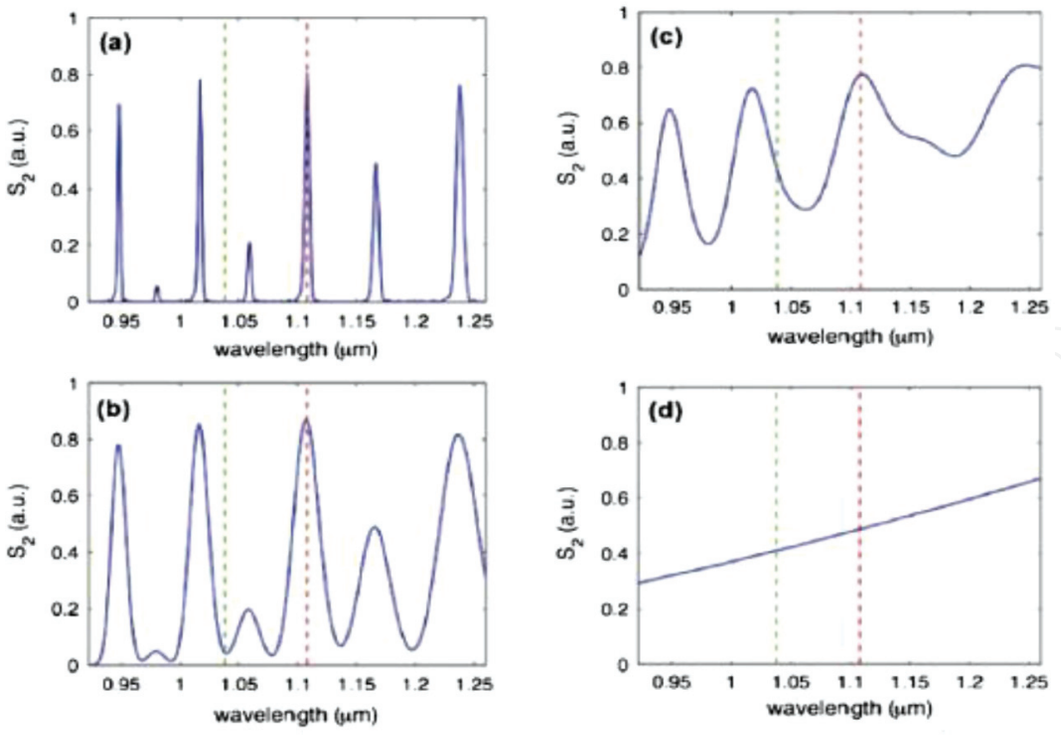

Figure 5. The spectral response of the Čerenkov SHG for different beam widths [28]. From (a) to (d), the beam widths of the fundamental wave are 60, 10, 5, and 2 μm, respectively. The plots are normalized to their individual maximum value.

In contrast to the Čerenkov emission defined by the fulfillment of the longitudinal phase-matching condition, the other group of the second harmonic diffraction spots (central spots located close to the pump in **Figure 4(a)**) only satisfies the transverse phase-matching (TPM) conditions, i.e., $\sin\theta_{RN} = mG_0/k_2$, for the mth diffraction order, m = 1,2,3… The external angles are then determined as follows:

$$\sin\beta_m = m\lambda_2/\Lambda,\ m = 1, 2, ..., \tag{6}$$

where λ_2 is the SH wavelength. This is a generic condition that holds for any periodic $\chi^{(2)}$ structure and does not depend on its refractive index.

The intensity of the nonlinear Raman-Nath second harmonic diffraction depends strongly on the duty cycle of the $\chi^{(2)}$ grating [29]. In fact the impact of the duty cycle on the nonlinear Raman-Nath diffraction is very similar to that in linear diffraction on dielectric grating. The duty cycle directly determines the Fourier coefficient g_m in Eq. (4), so it will cause the variation of the efficiency of nonlinear Raman-Nath diffraction. The detailed influence of duty cycle on the Raman-Nath diffraction from a periodic ($\Lambda = 9\ \mu m$) ferroelectric domain structure is shown in **Figure 6**. Agreeing quite well with the equation of Fourier coefficient $g_m(m \neq 0) = 2\sin(\pi mD)/\pi m$, the first-order Raman-Nath harmonic diffraction (m = 1) takes the maximum intensity at duty cycle D = 0.5, while the second-order (m = 1) exhibits two equal maxima at D = 0.25 and 0.75, respectively.

We consider now the influence of the structure randomness of ferroelectric domain patterns on the Raman-Nath harmonic diffraction. It is well known that the fabrication process of periodic domain patterns in ferroelectric crystals often introduces some degree of randomness in otherwise fully periodic domain structure. For the collinear quasi-phase-matching frequency conversion processes, the randomness generally has a negative impact because it reduces frequency conversion efficiency. The situation becomes more complicated when it comes to the nonlinear Raman-Nath diffraction. As we show in **Figure 7**, the randomness of the domain pattern not only affects the efficiency of nonlinear diffraction but also leads to appearance of

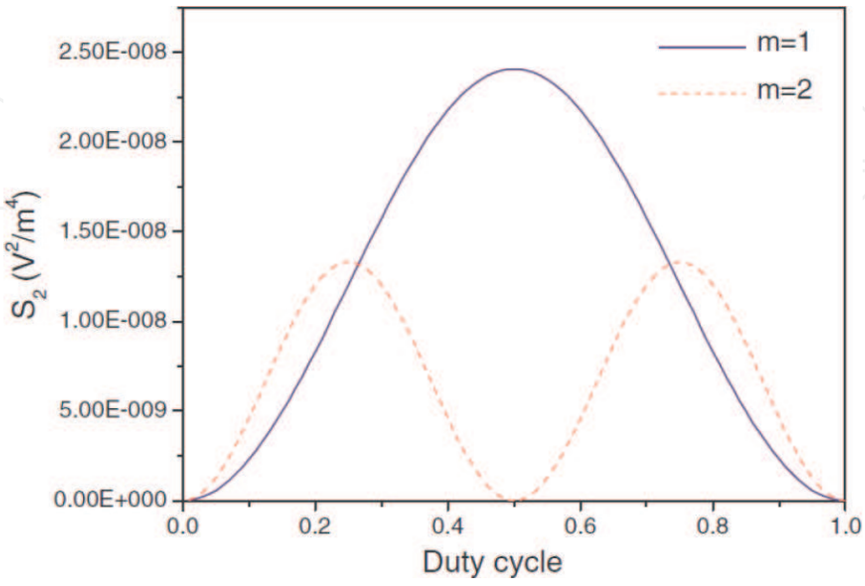

Figure 6. The effect of duty cycle on the strengths of nonlinear Raman-Nath diffraction [29].

http://dx.doi.org/10.5772/intechopen.77238

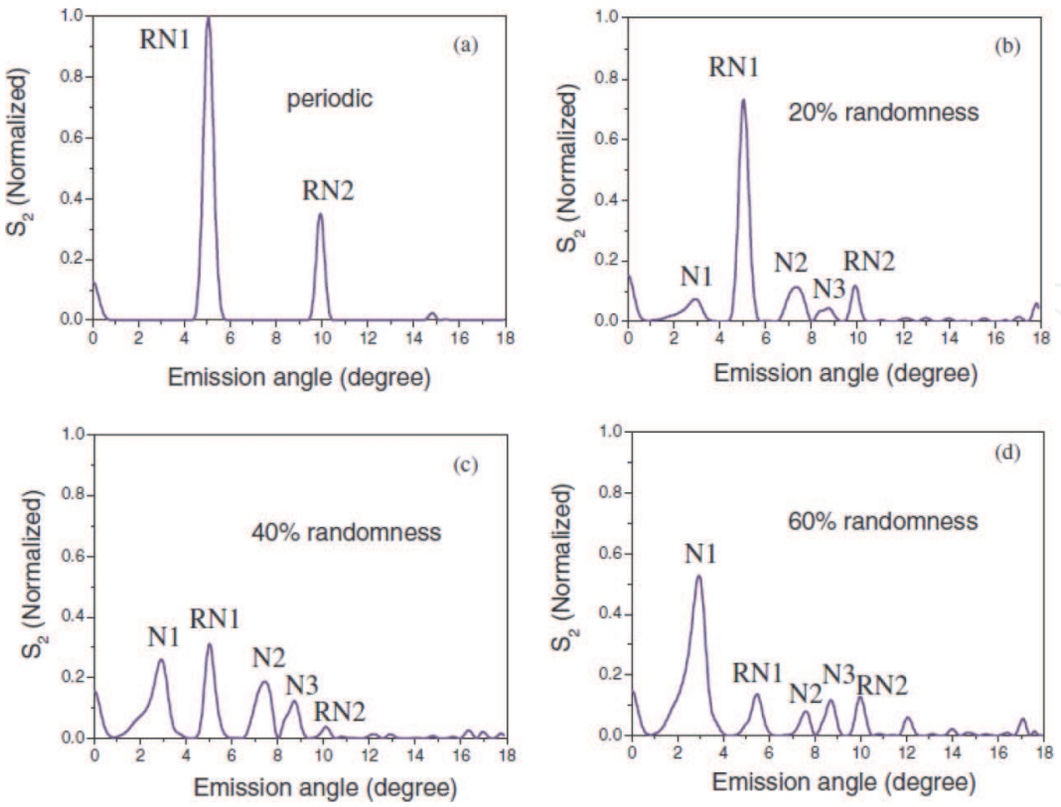

Figure 7. The influence of structure randomness of the ferroelectric domain patterns on the nonlinear Raman-Nath diffraction [29]. We take an average domain period $\Lambda_0 = 9$ m and consider four different degrees of structure randomness ranging from 0 to 60%. All emission strengths are normalized to that of the first-order Raman-Nath diffraction without randomness, namely, RN1 in (a).

new emission peaks. We choose an average period $\Lambda_0 = 9$ μm and consider that the domain width fluctuates randomly around its mean value. We consider four different degrees of randomness. From **Figure 7(a)–(d)**, the randomness degree increases from 0 to 60%, which is defined by $\sigma = \Delta l/\Lambda_0$ with Δl representing the largest dispersion of the ferroelectric domain width. In the figure, we show the normalized harmonic strengths with respect to that of the first-order nonlinear Raman-Nath diffraction without any randomness, namely, $\sigma = 0$. As shown in **Figure 7(a)**, two intensity maxima, which correspond, respectively, to the first- and second-order Raman-Nath resonances, appear for the perfect periodic structure. They are marked as RN1 and RN2 in the figure, respectively. Increasing σ leads to the weakening of these two emission peaks and at the same time appearance of a few new ones, marked with indices N1, N2, and N3 in **Figure 7(b)–(d)**. These new emitted signals become stronger and stronger with σ, and finally their strengths can exceed those of the original emission resonances.

In **Figure 8**, we display the calculated dependence of the nonlinear Raman-Nath diffractions on the interaction distance. As the Raman-Nath interactions suffer from the phase mismatch in the longitudinal direction, their intensity oscillates with the interaction distance inside the crystal. Obviously the smaller the phase mismatch, the longer the oscillation period. With the parameters used in our calculation (fundamental wavelength λ_1 = 1.545 μm, beam width a = 60 μm, duty cycle D = 0.35), the largest oscillation period takes place at the fifth-order diffraction (m = 5).

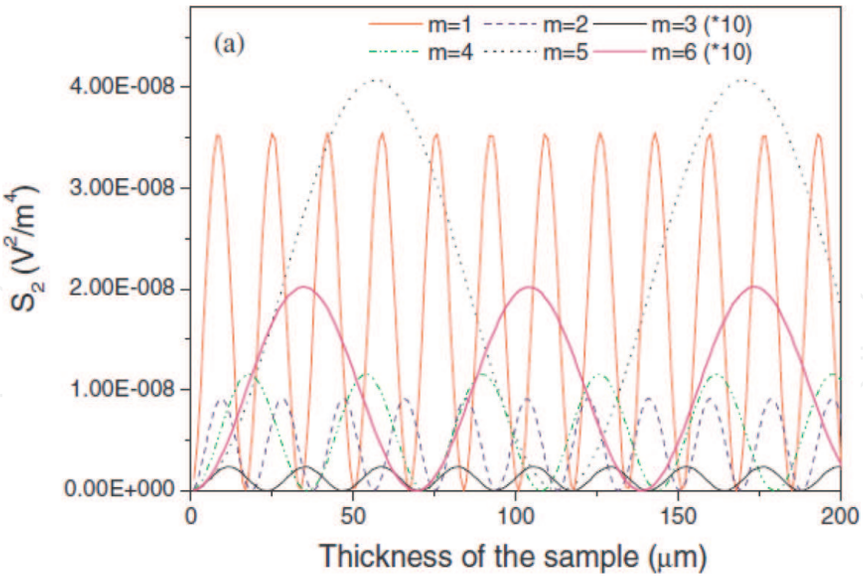

Figure 8. Multi-order nonlinear Raman-Nath SHG as a function of crystal thickness (or interaction distance) [29].

4. Application of Čerenkov harmonic generation to 3D imaging of ferroelectric domain patterns

High-quality visualization of ferroelectric domain structures plays a key role in understanding material property and better control of domain inversion process. However, due to the equality of antiparallel 180° ferroelectric domains in linear optical properties, the common imaging techniques do not apply to the detection of these domains. Currently the selective chemical etching [30] based on the different etching rates of antiparallel domains in hydrofluoric acid is still the most common method used for this purpose. Not only this is a destructive technique, but moreover, it is ineffective in revealing the internal domain structures hidden deep inside the crystals. To overcome some of these drawbacks, a large number of alternative approaches have been adapted to imaging ferroelectric domains, such as advanced electron microscopy [31] and piezo-forced microscopy [32]. However, most of these methods also fail in visualization of deep internal domain structures, which can be diverse and more complex than those on the surface [33]. For example, the inverted domains undergo sidewise expansion with depth [34], transform to preferred shapes depending on the crystallographic symmetry [35, 36], and sometimes merge to form a bigger structures [37]. The details about these domain formation processes such as when, where, and how they occur are very little known due to the lack of reliable techniques for three-dimensional visualization of domain patterns.

It has been shown in Section 2 that when a femtosecond laser beam is tightly focused to produce a focus that is narrow enough to cover a single ferroelectric domain wall, a pair of Čerenkov second harmonic beams will be generated. The Čerenkov signal disappears if the laser beam is moved away from the domain wall. In this way, by recording the second harmonic strengths at different positions inside the crystal, one can obtain a three-dimensional

image reflecting the spatial distribution of ferroelectric domain walls (and subsequently domains) inside the crystal. This is a nondestructive imaging method and can offer sub-micrometer resolution because of its nonlinear optical mechanism [18]. This is a 3D optical method as it also enables one to reveal the details of inverted domains beneath the surface.

Figure 9 displays a schematic illustration of the nonlinear Čerenkov second harmonic imaging system. The fundamental femtosecond laser beam is provided here by a titanium-sapphire laser (Mai Tai, Spectra Physics, 80 MHz repetition rate and up to 12 nJ pulse energy). It is known that in the regime of a tightly focused fundamental beam, the Čerenkov process is insensitive to the wavelength of the fundamental wave. Therefore, this imaging system can operate at a wide range of wavelength limited only by the absorption edge of second harmonic and the total reflection condition. The latter condition means the Čerenkov harmonic emission angle has to be smaller than its total reflection angle so that the Čerenkov signals can get out from the sample for detection. For traditional nonlinear optical ferroelectric materials, such as $LiNbO_3$ and $LiTaO_3$ crystals, the Čerenkov angle becomes larger at shorter wavelength, so the fundamental wavelength used for the visualization cannot be shorter than the critical wavelength.

The main part of this imaging system is a commercial laser scanning confocal microscope (Zeiss, LSM 510 + Axiovert 200). The femtosecond laser beam is coupled into the confocal microscope and then illuminates the sample after being tightly focused by an $100\times$ objective lens (Plan Apochromat, NA = 1.46). A pair of galvanometric mirrors is used to adjust the focus position in the X-Y plane, and a motorized stage is used to move the objective lens in the Z direction. To collect and detect the emitted second harmonic signal, a condenser lens and a

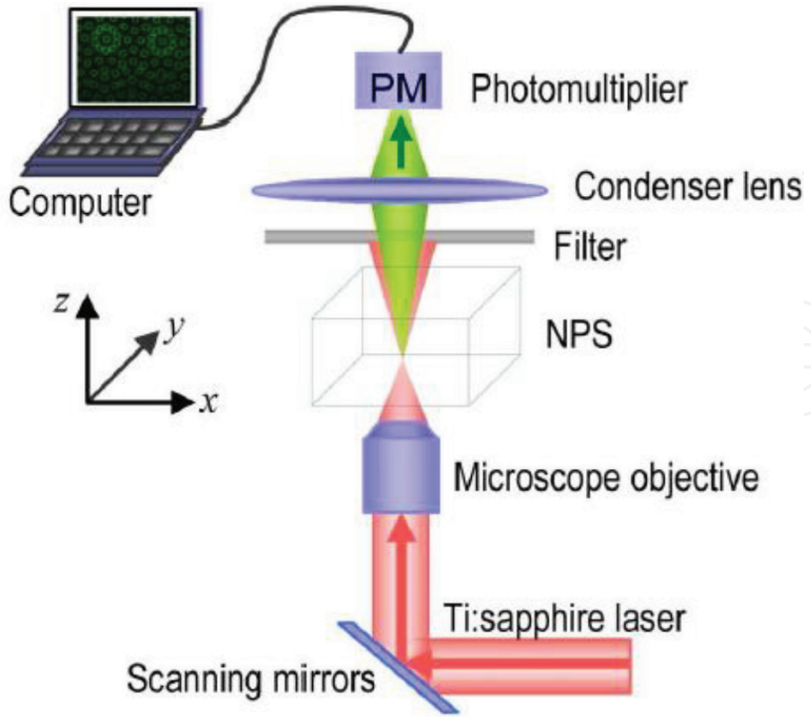

Figure 9. Schematic of the Čerenkov harmonic imaging system for visualization of ferroelectric domain patterns in a nonlinear photonic crystal (NPC) [18].

photomultiplier are employed, respectively. Short-pass filters are used to prevent the transmitted fundamental beam from entering the detectors.

The advantages of this nonlinear Čerenkov imaging system include:

4.1. High contrast and high spatial resolution

A typical two-dimensional image of a ferroelectric domain structure obtained by the Čerenkov second harmonic microscope is shown in **Figure 10(a)**. The quasi-periodic domain patterns, where the bright boundaries represent ferroelectric domain walls which facilitate stronger Čerenkov harmonic emissions, were clearly seen. Obviously the Čerenkov second harmonic microscope is capable of imaging ferroelectric domains with high contrast.

Figure 10(b) depicts the image of ferroelectric domain patterns obtained in an as-grown $Sr_{0.28}Ba_{0.72}Nb_2O_6$ crystal, which process naturally random domain structures in two dimensions. It is seen that the Čerenkov method offers an exceptional spatial resolution and even domain boundaries separated by less than 250 nm can be easily resolved. This is below the diffraction limit for the excitation laser wavelength of 820 nm, owing to the mechanism of nonlinear optical interaction, i.e., the Čerenkov second harmonic signal can only be excited in the very central part of the laser beam's focus.

4.2. Applicability to a wide range of materials

The imaging principle of the Čerenkov SHG microscope lies in the sensitivity of the Čerenkov emission on the existence of the spatial variation of the second-order nonlinearity $\chi^{(2)}$. Therefore, it can apply to any transparent materials with sharp $\chi^{(2)}$ variations. For example, in our experiment we have obtained high-quality images of ferroelectric domain patterns in $LiNbO_3$, $LiTaO_3$, $KTiOPO_4$, and $Sr_{0.28}Ba_{0.72}Nb_2O_6$ crystals, as shown in **Figure 11**.

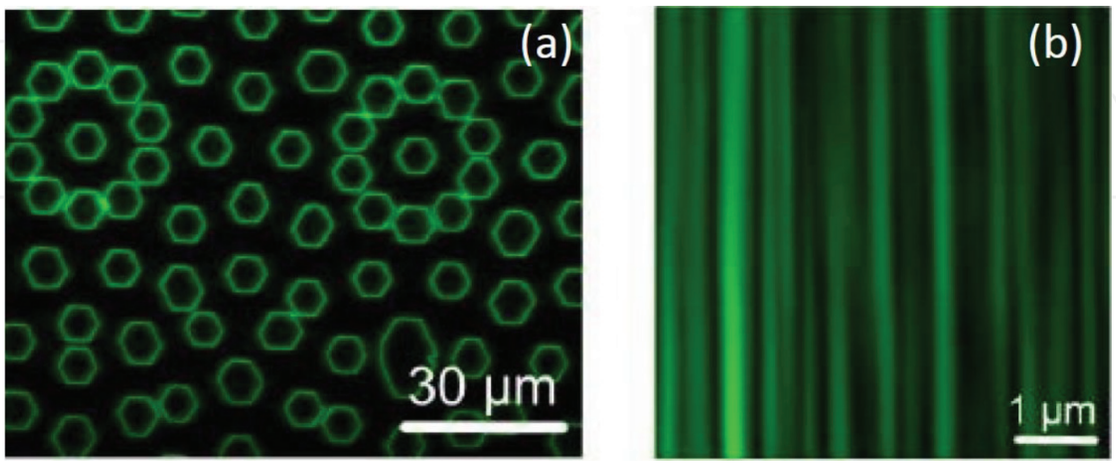

Figure 10. Domain structures imaged by Čerenkov SHG, taken with the focal plane of the fundamental beam located 10 mm inside the corresponding materials: (a) congruent $LiNbO_3$ with 2D quasi-periodic domain structure and (b) as-grown $Sr_{0.28}Ba_{0.72}Nb_2O_6$ crystal.

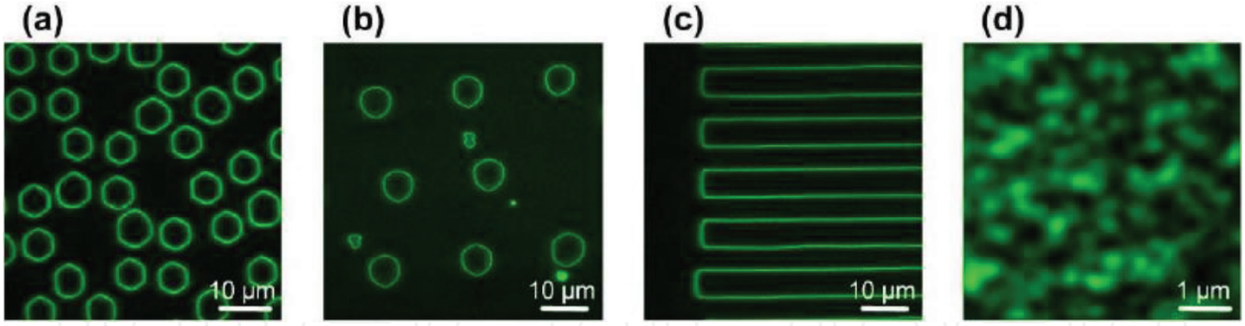

Figure 11. The Čerenkov SHG microscopy applies to a wide range of ferroelectric materials [18]. (a) Congruent $LiNbO_3$ with 2D short-range-ordered domain structure [38]. (b) Stoichiometric $LiTaO_3$ with 2D quasi-periodic domain structure [39]. (c) $KTiOPO_4$ with 1D periodic domain structure [40]. (d) z-cut as-grown $Sr_{0.28}Ba_{0.72}Nb_2O_6$ crystal with naturally random domain structure at X-Y plane [41].

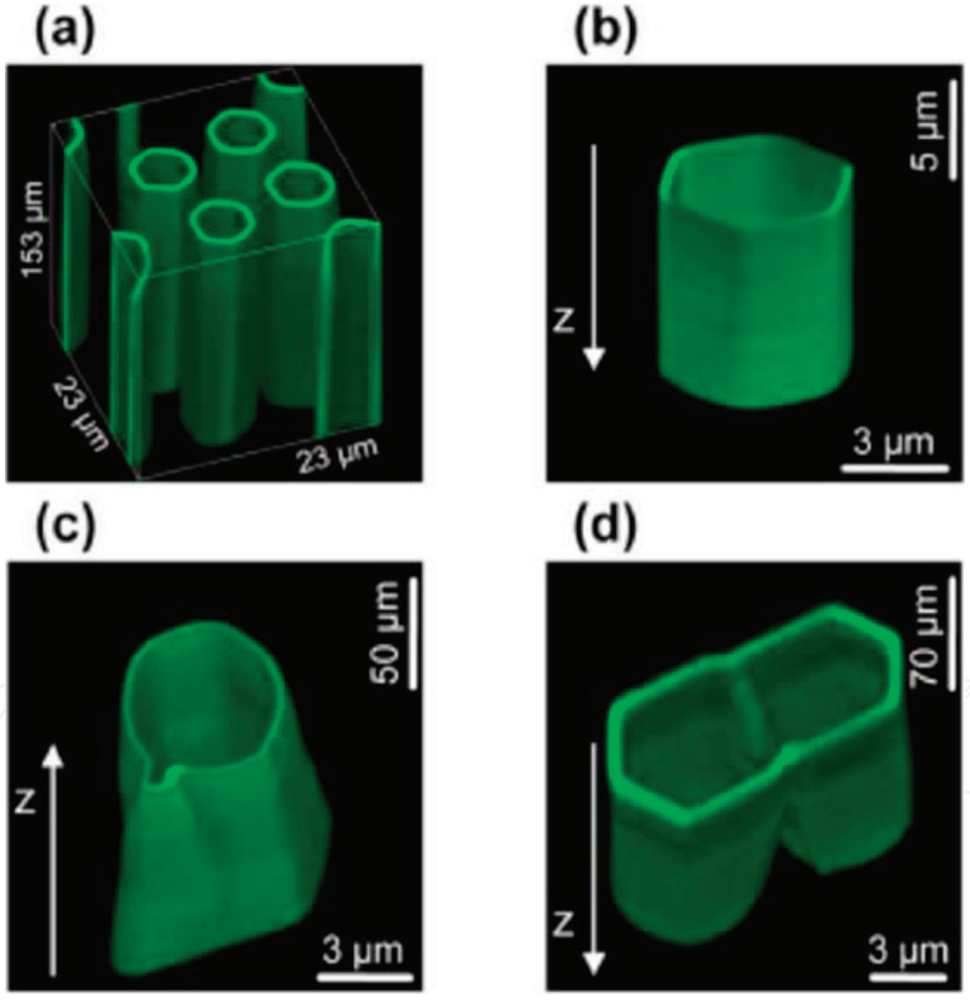

Figure 12. Three-dimensional visualization of inverted ferroelectric domains inside congruent $LiNbO_3$ crystal by Čerenkov-type second harmonic generation laser scanning microscopy. (a) Domain distribution in the nonlinear photonic structure. (b) Transformation from the initially circular to hexagonally shaped domains. (c) Formation of a defect during the domain growth. (d) Merging of two initially separated ferroelectric domains. The ImageJ software was used to create these images.

4.3. Capability for 3D imaging

As we described above, the scanning of laser focus in the X-Y plane enables us to obtain two-dimensional images of ferroelectric domains. Then if we stack a series X-Y plane images recorded at different depths inside the material, we can produce 3D images of domains. This is an advantage that cannot be met by the traditional domain imaging techniques. In **Figure 12** we show a number of 3D images of ferroelectric domain patterns, which are formed in a congruent $LiNbOb_3$ crystal [38]. From these images we can see how the initially circular-shaped domains transform to hexagons with depth [**Figure 12(b)**], how defects were formed during the domain inversion process [**Figure 12(c)**], and how the neighboring domains merge to form a bigger one [**Figure 12(d)**]. Revealing these details is essential for a full understanding of domain inversion and growth processes. This is also very useful for improving the quality of ferroelectric domain patterns, which is critical for a wide range of future applications.

5. Conclusion

We have investigated the nonlinear optical interactions that are strongly dependent on the existence of ferroelectric domain walls, i.e., the spatial variation of the second-order nonlinear coefficient $\chi^{(2)}$ In particular, we have discussed the so-called nonlinear Čerenkov radiation focusing on two special cases including the signal generation from a single and multiple ferroelectric domain wall(s). We have shown that the localized spatial change of nonlinearity $\chi^{(2)}$ constitutes a sufficient condition for strong Čerenkov second harmonic generation. The emitted Čerenkov signals arising from multiple walls can interfere with each other, resulting in the strong dependence of the strength of the overall Čerenkov beams on the wavelengths. Furthermore, the emission from regular periodic domain pattern gives rise to another type of nonlinear interaction, namely, the nonlinear Raman-Nath diffraction. We have derived analytical formulas that govern the emission process and discussed factors that influence the strength of the nonlinear diffraction, including the duty cycle, thickness of the crystal, randomness in domain size, as well as the beam width and wavelength of the fundamental wave. We also utilized the effect of Čerenkov second harmonic generation from a single-domain wall for direct 3D imaging of the antiparallel domains in ferroelectric crystals with sub-diffraction limit resolution. Our studies are important for a better understanding of nonlinear diffraction from ferroelectric domain structures. The nonlinear optical microscopy forms a very powerful tool that will further inspire the design and development of new and sophisticated ferroelectric domain structures for advanced photonic applications.

Acknowledgements

The authors thank the Australian Research Council and Qatar National Research Fund (Grant No. NPRP 8-246-1-060) for financial supports. Mr. Xin Chen thanks China Scholarship Council (PhD Scholarship No. 201306750005). The authors thank Dr. Vito Roppo, Dr. Ksawery

Kalinowski, Dr. Qian Kong, Dr. Wenjie Wang, Prof. Crina Cojocaru, and Prof. Joes Trull for their valued contributions to this work.

Conflict of interest

There is no conflict of interest for this work.

Author details

Xin Chen[1], Wieslaw Krolikowski[1,2] and Yan Sheng[1]*

*Address all correspondence to: yan.sheng@anu.edu.au

1 Laser Physics Centre, Research School of Physics and Engineering, Australian National University, Canberra, Australia

2 Science Program, Texas A&M University at Qatar, Doha, Qatar

References

[1] Valasek J. Piezo-electric and allied phenomena in rochelle salt. Physics Review. 1921;**17**: 475-481. DOI: 10.1103/PhysRev.17.475

[2] Matsumoto S, Lim EJ, Hertz HM, Fejer MM. Quasiphase-matched second harmonic generation of blue light in electrically periodically-poled lithium tantalate waveguides. Electronics Letters. 1991;**27**:2040-2042. DOI: 10.1049/el:19911263

[3] Burns WK, McElhanon W, Goldberg L. Second harmonic generation in field poled, quasi-phase-matched, bulk $LiNbO_3$. IEEE Photonics Technology Letters. 1994;**6**:252-254. DOI: 10.1109/68.275441

[4] Catalan G, Seidel J, Ramesh R, Scott JF. Domain wall nanoelectronics. Reviews of Modern Physics. 2012;**84**:119-156. DOI: 10.1103/RevModPhys.84.119

[5] Seidel J, Fu D, Yang S, Alarcón-Lladó E, Wu J, Ramesh R, Ager JW III. Efficient photovoltaic current generation at ferroelectric domain walls. Physical Review Letters. 2011;**107**: 126805. DOI: 10.1103/PhysRevLett.107.126805

[6] Scott JF, Paz de Araujo CA. Ferroelectric memorie. Science. 1989;**246**:1400-1405. DOI: 10.1126/science.246.4936.1400

[7] Guo R, You L, Zhou Y, Lim ZS, Zou X, Chen L, Ramesh R, Wang J. Non-volatile memory based on the ferroelectric photovoltaic effect. Nature Communications. 2013;**4**:1990. DOI: 10.1038/ncomms2990

[8] Cho Y, Fujimoto K, Hiranaga Y, Wagatsuma Y, Onoe A, Terabe K, Kitamura K. Terabit inch^{-2} ferroelectric data storage using scanning nonlinear dielectric microscopy nanodomain engineering system. Nanotechnology. 2003;**14**:637-642. DOI: 10.1088/0957-4484/14/6/314

[9] Ito H, Takyu C, Inaba H. Fabrication of periodic domain grating in $LiNbO_3$ by electron beam writing for application of nonlinear optical processes. Electronics Letters. 1991;**27**: 1221-1222. DOI: 10.1049/el:19910766

[10] Chen X, Shvedov V, Karpinski P, Sheng Y, Koynov K, Boes A, Mitchell A, Trull J, Cojocaru C, Krolikowski W. Ferroelectric domain patterning with ultrafast light. Optics & Photonics News. 2016;**27**:50

[11] Chen X, Karpinski P, Shvedov V, Koynov K, Wang B, Trull J, Cojocaru C, Krolikowski W, Sheng Y. Ferroelectric domain engineering by focused infrared femtosecond pulses. Applied Physics Letters. 2015;**107**:141102. DOI: 10.1063/1.4932199

[12] Chen X, Karpinski P, Shvedov V, Boes A, Mitchell A, Krolikowski W, Sheng Y. Quasi-phase matching via femtosecond laser-induced domain inversion in lithium niobate waveguides. Optics Letters. 2016;**41**:2410-2413. DOI: 10.1364/OL.41.002410

[13] Ying CYJ, Muir AC, Valdivia CE, Steigerwald H, Sones CL, Eason RW, Soergel E, Mailis S. Light-mediated ferroelectric domain engineering and micro-structuring of lithium niobate crystals. Laser & Photonics Reviews. 2012;**6**:526-548. DOI: 10.1002/lpor.201100022

[14] Sheng Y, Roppo V, Kalinowski K, Krolikowski W. Role of a localized modulation of (χ(2)) in Čerenkov second-harmonic generation in nonlinear bulk medium. Optics Letters. 2012; **37**:3864-3866. DOI: 10.1364/OL.37.003864

[15] Roppo V, Kalinowski K, Sheng Y, Krolikowski W, Cojocaru C, Trull J. Unified approach to Čerenkov second harmonic generation. Optics Express. 2013;**21**:25715. DOI: 10.1364/OE.21.025715

[16] Deng X, Chen X. Domain wall characterization in ferroelectrics by using localized nonlinearitie. Optics Express. 2010;**18**:15597-15602. DOI: 10.1364/OE.21.025715

[17] Saltiel SM, Sheng Y, Voloch-Bloch N, Neshev DN, Krolikowski W, Arie A, Koynov K, Kivshar YS. Cerenkov-type second-harmonic generation in two-dimensional nonlinear photonic structures. IEEE Journal of Quantum Electronics. 2009;**45**:1465-1472. DOI: 10.1109/JQE.2009.2030147

[18] Sheng Y, Best A, Butt H, Krolikowski W, Arie A, Koynov K. Three-dimensional ferroelectric domain visualisation by Čerenkov-type second harmonic generation. Optics Express. 2010;**18**:16539-16545. DOI: 10.1364/OE.18.016539

[19] Karpinski P, Chen X, Shvedov V, Hnatovsky C, Grisard A, Lallier E, Luther-Davies B, Krolikowski W, Sheng Y. Nonlinear diffraction in orientation-patterned semiconductors. Optics Express. 2013;**25**:14903-14912. DOI: 10.1364/OE.23.014903

[20] Wang B, Cojocaru C, Krolikowski W, Sheng Y, Trull J. Transverse single-shot cross-correlation scheme for laser pulse temporal measurement via planar second harmonic generation. Optics Express. 2016;**24**:22210-22218. DOI: 10.1364/OE.24.022210

[21] Chen X, Switkowski K, Hu X, Krolikowski W, Sheng Y. Enhanced fourth harmonic generation via nonlinear erenkov interaction in periodically poled lithium niobate crystal. Optics Express. 2016;**24**:29948-29954. DOI: 10.1364/OE.24.029948

[22] Ayoub M, Futterlieb H, Imbrock J, Denz C. 3D imaging of ferroelectric kinetics during electrically driven switching. Advanced Materials. 2017;**29**:1603325. DOI: 10.1002/adma.201603325

[23] Boyd RW. Nonlinear Optics. New York: Academic Press; 2007

[24] Edwards GJ, Lawrence M. A temperature-dependent dispersion equation for congruently grown lithium niobate. Optical and Quantum Electronics. 1984;**16**:373-375. DOI: 10.1007/BF00620081

[25] Mathieu E. Conditions for quasi Cerenkov radiation, generated by optical second harmonic polarisation in a nonlinear crystal. Zeitschrift für Angewandte Mathematik und Physik. 1969;**20**:433-439. DOI: 10.1007/BF01595035

[26] Wulle T, Herminghaus S. Nonlinear optics of Bessel beams. Physical Review Letters. 1993;**70**:1401-1404. DOI: 10.1103/PhysRevLett.70.1401

[27] Saltiel SM, Neshev DN, Fischer R, Krolikowski W, Arie A, Kivshar YS. Generation of second-harmonic conical waves via nonlinear Bragg diffraction. Physical Review Letters. 2008;**100**:103902. DOI: 10.1103/PhysRevLett.100.103902

[28] Sheng Y, Kong Q, Roppo V, Kalinowski K, Wang Q, Cojocaru C, Krolikowski W. Theoretical study of Čerenkov-type second-harmonic generation in periodically poled ferroelectric crystals. Journal of the Optical Society of America B: Optical Physics. 2012;**29**:312-318. DOI: 10.1364/JOSAB.29.000312

[29] Sheng Y, Kong Q, Wang W, Kalinowski K, Krolikowski W. Theoretical investigations of nonlinear Raman–Nath diffraction in the frequency doubling process. Journal of Physics B: Atomic, Molecular and Optical Physics. 2012;**45**:055401. DOI: 10.1088/0953-4075/45/5/055401

[30] Hooton JA, Merz WJ. Etch patterns and ferroelectric domains in $BaTiO_3$ single crystal. Physical Review. 1955;**98**:409-413. DOI: 10.1103/PhysRev.98.409

[31] Zhu SN, Cao WW. Direct observation of ferroelectric domains in $LiTaO_3$ using environmental scanning electron microscopy. Physical Review Letters. 1997;**79**:2558-2561. DOI: 10.1103/PhysRevLett.79.2558

[32] Jungk T, Hoffmann A, Soergel E. Contrast mechanisms for the detection of ferroelectric domains with scanning force microscopy. New Journal of Physics. 2009;**11**:033092. DOI: 10.1088/1367-2630/11/3/033029

[33] Soergel E. Visualization of ferroelectric domains in bulk single crystals. Applied Physics. 2005;**81**:729-752. DOI: 10.1007/s00340-005-1989-9

[34] Shur VY, Rumyantsev EL, Batchko RG, Miller GD, Fejer MM, Byer RL. Domain kinetics in the formation of a periodic domain structure in lithium niobate. Physics of the Solid State. 1999;**41**:1681-1687. DOI: 10.1134/1.1131068

[35] Rosenman G, Garb K, Skliar A, Oron M, Eger D, Katz M. Domain broadening in quasi-phase-matched nonlinear optical devices. Applied Physics Letters. 1998;**73**:865-867. DOI: 10.1063/1.121969

[36] Sheng Y, Wang T, Ma BQ, Qu E, Cheng B, Zhang D. Anisotropy of domain broadening in periodically poled lithium niobate crystal. Applied Physics Letters. 2006;**88**:041121. DOI: 10.1063/1.2168727

[37] Ni PG, Ma BQ, Wang XH, Cheng B, Zhang D. Second-harmonic generation in two-dimensional periodically poled lithium niobate using second-order quasiphase matching. Applied Physics Letters. 2003;**82**:4230-4232. DOI: 10.1063/1.1579856

[38] Sheng Y, Dou J, Ma B, Cheng B, Zhang D. Broadband efficient second harmonic generation in media with a short-range order. Applied Physics Letters. 2007;**91**:011101. DOI: 10.1063/1.2754365

[39] Bahabad A, Ganany-Padowicz A, Arie A. Engineering two-dimensional nonlinear photonic quasi-crystal. Optics Letters. 2008;**33**:1386-1388. DOI: 10.1364/OL.33.001386

[40] Ni R, Du L, Wu Y, Hu XP, Zou J, Sheng Y, Arie A, Zhang Y, Zhu SN. Nonlinear Cherenkov difference-frequency generation exploiting birefringence of KTP. Applied Physics Letters. 2016;**108**:031104. DOI: 10.1063/1.4940095

[41] Fischer R, Saltiel SM, Neshev DN, Krolikowski W, Kivshar YS. Broadband femtosecond frequency doubling in random media. Applied Physics Letters. 2006;**89**:191105. DOI: 10.1063/1.2374678